ChemComm

COMMUNICATION

Cite this: *Chem. Commun.*, 2021, 57, 4182

Received 8th February 2021, Accepted 16th March 2021

DOI: 10.1039/d1cc00701g

rsc.li/chemcomm

$BaB_4O_5F_4$ with reversible phase transition featuring unprecedented fundamental building blocks of $[B_{16}O_{21}F_{16}]$ in the α-phase and $[B_4O_6F_4]$ in the β-phase†

Wenbin Zhang,‡[ab] Siru Guo,‡[ab] Shujuan Han, *[ab] Liying Wang,[c] Xin Zhou,[c] Zhihua Yang[ab] and Shilie Pan *[ab]

The first fluorooxoborate with reversible phase transition, $BaB_4O_5F_4$, has been obtained. Interestingly, the two polymorphs, α- and β-$BaB_4O_5F_4$ with rare $[BOF_3]$, feature various one-dimensional chains composed of the unprecedented fundamental building blocks of $[B_{16}O_{21}F_{16}]$ and $[B_4O_6F_4]$, respectively. First-principles calculations were performed to elucidate the structure–property relationships.

With structural versatility, a wide transmittance range, and a high laser damage threshold, borates are the preferred system for probing optical crystals, and they have highly significant applications in semiconductor manufacturing, laser micromachining, photolithography, and other aspects.[1] As the basic structural building blocks of borate, triangular $[BO_3]$ or tetrahedral $[BO_4]$ can be interconnected by sharing O atoms to form different fundamental building blocks (FBBs), such as $[B_3O_6]$ in β-BaB_2O_4,[2] $[B_{11}O_{22}]$ in $Li_6Rb_5(B_{11}O_{22})$,[3] $[B_{63}O_{133}]$ in $Cs_3B_7O_{12}$,[4] and $[B_{40}O_{77}]$ in $Li_4Cs_4B_{40}O_{64}$,[5] *etc.* Then, the interconnection of each FBB results in the borates exhibiting multiple anionic frameworks: isolated clusters, one-dimensional (1D) infinite chains, 2D layers, or 3D frameworks.[6] These results greatly enrich the structural chemistry of borates.

Furthermore, the introduction of F atoms with large electronegativity can result in the structural chemistry of borate being more abundant, especially as fluorooxoborate with the B–F bond is formed.[7] In general, F can substitute the O atom in $[BO_4]$ to form $[BO_3F]$, $[BO_2F_2]$, and $[BOF_3]$ groups. Up until now, $[BO_3F]$ and $[BO_2F_2]$ groups have been present in most fluorooxoborates, while $[BOF_3]$ groups are extremely rare. The $[BO_xF_{4-x}]$ (x = 1, 2, and 3) basic units are further interconnected by $[BO_3]$ or $[BO_4]$ to form novel FBBs, such as $[B_2O_6F]$ in BiB_2O_4F,[8] $[B_4O_8F]$ in AB_4O_6F (A = NH_4, Na, Rb, Cs, K/Cs, or Rb/Cs),[9] $[B_7O_{13}F_2]$ in $Na_3B_7O_{11}F_2$,[10] *etc.*, and these further enrich the diversity of the B–O–F anion framework. In addition, F as the terminal atom facilitates breaking of the 3D B–O network structure, resulting in it being more inclined to form various 2D, 1D or isolated structures.[11] Moreover, most of the B–O–F anionic frameworks exhibit isolated clusters and 2D layer structures, and only very few of them present 1D chain structures.[12] The 1D chain structure may twist under certain circumstances, producing a phase transition. In addition, polymorphism is of particular interest and is important for developing new functional materials and understanding structure–property relationships, since polymorphism has promising applications in pharmaceuticals, pigments, foods, dyestuffs and so on.[13] In addition to enriching the structural chemistry, fluorooxoborates have also received much attention in recent years for their excellent performance induced by the $[BO_xF_{4-x}]$ groups. Compared with $[BO_3]$ and $[BO_4]$, the larger hyper-polarizability tensor and highest occupied molecular orbital-lowest unoccupied molecular orbital (HOMO–LUMO) gaps of the $[BO_xF_{4-x}]$ groups can result in enhanced anisotropy, as well as blue-shift the cut-off edge.[14] Fluorooxoborate is one of the prominent research topics in the exploration of new deep ultraviolet (DUV) optical crystals.

In this communication, we have discovered the first case among alkaline earth metal fluorooxoborates to exhibit reversible phase transition, $P2_1$ for α-$BaB_4O_5F_4$, and $P2_1/c$ for β-$BaB_4O_5F_4$ (α and β correspond to low and high temperature phases, respectively). α-$BaB_4O_5F_4$ and β-$BaB_4O_5F_4$ exhibit 1D chains composed of unprecedented FBBs, $[B_{16}O_{21}F_{16}]$ and $[B_4O_6F_4]$, respectively. The crystallographic data and details of

[a] *CAS Key Laboratory of Functional Materials and Devices for Special Environments, Xinjiang Technical Institute of Physics & Chemistry, CAS, Xinjiang Key Laboratory of Electronic Information Materials and Devices, 40-1 South Beijing Road, Urumqi 830011, China. E-mail: hansj@ms.xjb.ac.cn, slpan@ms.xjb.ac.cn*
[b] *Center of Materials Science and Optoelectronics Engineering, University of Chinese Academy of Sciences, Beijing 100049, China*
[c] *Key Laboratory of Magnetic Resonance in Biological Systems, State Key Laboratory of Magnetic Resonance and Atomic and Molecular Physics, National Center for Magnetic Resonance in Wuhan, Wuhan Institute of Physics and Mathematics, CAS, Wuhan 430071, P. R. China*

† Electronic supplementary information (ESI) available: Synthesis, crystallographic studies, characterization, and computational descriptions. CCDC 2059274 and 2059273 for α- and β-$BaB_4O_5F_4$. For ESI and crystallographic data in CIF or other electronic format see DOI: 10.1039/d1cc00701g

‡ These authors contributed equally to this work.

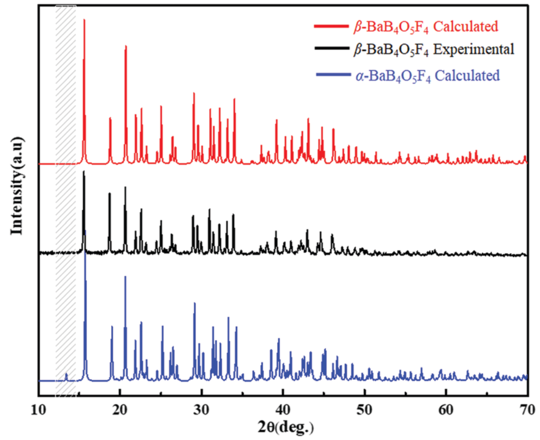

Fig. 1 The calculated powder X-ray diffraction patterns for α- and β-$BaB_4O_5F_4$, and the experimental powder X-ray diffraction patterns for β-$BaB_4O_5F_4$.

the structural refinement of α- and β-$BaB_4O_5F_4$ are provided in Tables S1–S4 in the ESI.†

Single crystal X-ray diffraction revealed that the two new compounds crystallized into the space groups of $P2_1$ (No. 4) and $P2_1/c$ (No. 14), respectively (Table S5, ESI†). Relatively low temperature and the residual factor validated models of these two crystals indicated the presence of two polymorphs. By comparing the standard XRD of the $BaB_4O_5F_4$ polymorphs, it is clear that the theoretical XRD pattern of α-$BaB_4O_5F_4$ has one obvious peak at $2\theta = 13.5°$ (Fig. 1). The polycrystalline sample of β-$BaB_4O_5F_4$ was obtained at 450 °C in the closed system. In order to further explore the temperature of its phase transition, the polycrystalline sample was tested using a Bruker SMART APEX II CCD under the temperatures of 295, 250, 220, 200, and 190 K (Fig. S1, ESI†). β-$BaB_4O_5F_4$ was stable from room temperature to 220 K, and then it begins to change into α-$BaB_4O_5F_4$ in the temperature range from 220 to 190 K. When the temperature begins to rise, the α-$BaB_4O_5F_4$ phase can also change into β-$BaB_4O_5F_4$ (the appearance of the X-ray diffraction peaks at about $2\theta = 13.5°$ can help us to judge this phase transition), indicating the reversibility of this phase transition.

α-$BaB_4O_5F_4$ crystallizes in the monoclinic space group $P2_1$ with four unique barium sites, sixteen unique boron sites, twenty unique oxygen sites, and sixteen unique fluorine sites in the asymmetric structure unit. β-$BaB_4O_5F_4$ crystallizes in the centrosymmetric space group, $P2_1/c$. There are one, four, five, and four crystallographically-independent atom numbers for Ba, B, O, and F in the asymmetric structure unit, respectively. Both α and β-$BaB_4O_5F_4$ exhibit a 3D framework composed of [BO_3], [BO_3F], [BOF_3] and [BaO_5F_6] groups. In α-$BaB_4O_5F_4$, four [B_3O_6F] rings are linked together by sharing vertex O atoms to form a [$B_{12}O_{21}F_4$] short chain, which further connects four [BOF_3] units to build its FBB, [$B_{16}O_{21}F_{16}$]. Then, the FBBs are linked together to construct the 1D [$B_{16}O_{20}F_{16}$]$_\infty$ chains, and the Ba cations are sequentially distributed among the chains to maintain the structural balance (Fig. 2b). Compared with α-$BaB_4O_5F_4$, β-$BaB_4O_5F_4$ features different 1D [$B_4O_5F_4$]$_\infty$ chains that are separated by Ba atoms, and its FBB is [$B_4O_6F_4$] composed of one [B_3O_6F] unit and one [BOF_3] unit. The structural difference between α- and β-$BaB_4O_5F_4$ is shown in Fig. 2, there are four types of [BOF_3] in α-$BaB_4O_5F_4$, and only one unique [BOF_3] group in β-$BaB_4O_5F_4$. It can clearly be observed that the four types of [BOF_3] tetrahedra are arranged alternately in the chain, which shows the different orientations in α-$BaB_4O_5F_4$, while the [BOF_3] groups in β-$BaB_4O_5F_4$ are arranged in two directions along the *c*-axis. As shown in Fig. S2 (ESI†), in α-$BaB_4O_5F_4$, the [$B_{16}O_{20}F_{16}$]$_\infty$ chain can generate itself only by 2_1-screw axes. For β-$BaB_4O_5F_4$, as well as the 2_1-screw axes, a glide plane is added, seen from the *a*-axes, the BO_3F group (1) operates itself by a mirror symmetrical

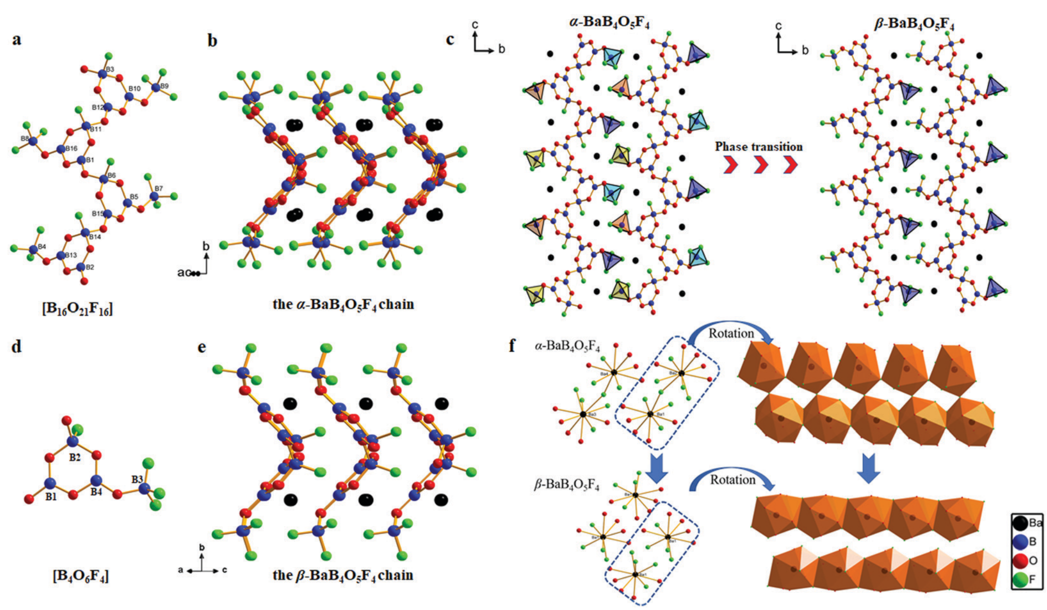

Fig. 2 The crystal structure features of $BaB_4O_5F_4$. (a and d) The FBB of α- and β-$BaB_4O_5F_4$. (b, c, e and f) The structure differences between α- and β-$BaB_4O_5F_4$.

operation, and then shifts a distance of $c/2$ to generate the BO_3F group (2). Eventually, β-$BaB_4O_5F_4$ crystallizes in the $P2_1/c$ symmetry group.

In α-$BaB_4O_5F_4$, the B (1, 2, 5, 10, 12, 13, 15, and 16) atoms are coordinated with three O atoms, forming [BO_3] units with B–O bond lengths varying from 1.291 to 1.412 Å, respectively, while B (3, 6, 11, and 14) atoms and B (4, 7, 8, and 9) atoms are located in the four-coordination environment to form the [BO_3F] and [BOF_3] units, respectively (the B–F bond lengths vary from 1.363 to 1.457 Å). However, in β-$BaB_4O_5F_4$, B(1 and 4)O_3, B(2)O_3F and B(3)OF_3 are connected, resulting in a six-membered ring structure, [$B_4O_6F_4$] (Fig. 2d). The B–O bond lengths are in the range of 1.353–1.458 Å, and the B–F bond lengths range from 1.364 to 1.432 Å, which are consistent with the previously reported results in the borate system.

In addition, the Ba cations are coordinated with five O atoms and six F atoms to form [BaO_5F_6] polyhedra in α- and β-$BaB_4O_5F_4$. Due to the change in the B–O–F chains, there is also a difference in the arrangement of cations. In α-$BaB_4O_5F_4$, the Ba(1)–O chain, which is formed by Ba(1)O_5F_6, further links with the Ba(2)–O chain by sharing F atoms, to give the Ba–O–F double chain, and the Ba (3 and 4) cations also exhibit the same arrangement. Compared with α-$BaB_4O_5F_4$, the unique [BaO_5F_6] polyhedron is connected with each other by sharing F atoms to form a 1D single chain in β-$BaB_4O_5F_4$ (Fig. 2f). In addition, the calculated bond valence sum (BVS) values of these atoms are shown in Tables S1 and S3 (ESI†),[15] and these values are within the allowable range, proving the accuracy of the structures. The Global Instability Index (GII) was also calculated,[16] which is derived from the bond valence concepts and can be used to evaluate the rationality of structures. Values greater than 0.05 valence units (vu) indicate that the structure is strained, whereas values greater than 0.20 vu indicate that the strain is so great that the structure is unstable. The calculated GII values of α- and β-$BaB_4O_5F_4$ are in the range of 0.089–0.093 vu (Table 1). The values of bond valence and GII for the two compounds are reasonable, suggesting that the crystal structures of these compounds are reasonable.

It is worth noting that the FBBs of α- and β-$BaB_4O_5F_4$ have never been reported in previously reported fluorooxoborates. To the best of our knowledge, 21 different FBBs have been reported in fluorooxoborates,[12c,17] the title compounds were firstly discovered with [BOF_3] groups in the fluorooxoborate without the hydroxyl, and [BOF_3] groups were also found in $Ba(B_2OF_3(OH)_2)_2$.[18] In addition, the FBBs of other fluorooxoborates with four B atoms in the molecular formula, AB_4O_6F (A = NH_4 and alkali metal), $AB_4O_6F_2$ (A = Ca, Sr, and Ba),[19] and $KNiB_4O_6F_3$,[20] were composed of [BO_3] and [BO_3F], as listed in Fig. S3 (ESI†). All of these FBBs form 2D B–O–F anion layered structures. Furthermore, from a molecular formula point of view, $BaB_4O_5F_4$ can be seen as two F atoms replacing one O atom in $BaB_4O_6F_2$. As more fluorine atoms are introduced into the structure, some of them as terminal atoms could break the original 18-membered ring in the $BaB_4O_6F_2$ structure, as a scissor. Then, the layered framework (2D) is destroyed, to form the chain (1D) in $BaB_4O_5F_4$, thereby further enriching the diversity of fluorooxoborate structures.

In order to confirm the presence of F atoms, energy dispersive X-ray spectroscopy (EDS) was carried out on the clean single crystal surface, and the results revealed the presence of F and O atoms in $BaB_4O_5F_4$ (Fig. S4, ESI†). Solid state Nuclear Magnetic Resonance (NMR) spectroscopy was carried out to verify the existence of B–F bonds. In the ^{19}F MAS NMR spectrum, the signals at −120.1 and −122.2 ppm were assigned to the F atoms in the B–F groups (Fig. 3a).[18,21] For the ^{11}B MAS NMR spectrum, according to previous work, the broad signals within the range of 5 to 15 ppm can be assigned to the chemical shifts of BO_3 units, and the narrow signals around 0 ppm can be assigned to the tetrahedral coordinated B atoms.[22] The ^{11}B{^{19}F}-rotational echo double resonance (REDOR) experiments were performed to establish the B–F bonds for the tetrahedral [BO_3F] and [BOF_3] units, and the differences in the obtained spectra are shown in Fig. 3c, which clearly indicates the existence of tetrahedrally coordinated B nuclei with B–F bonds in β-$BaB_4O_5F_4$. The IR spectrum of the β-$BaB_4O_5F_4$ compound is shown in Fig. S5 (ESI†). The peak assignments are comparable to those of previously reported fluorooxoborates, proving the correctness and reliability of the structure. The UV-vis-NIR diffuse-reflectance data was collected for the as-synthesized β-$BaB_4O_5F_4$ compound, and the data indicated that the compound has a wide transparent region and the bandgap is larger than 6.72 eV (Fig. S6, ESI†).

To investigate the relationship between the structure and properties of α- and β-$BaB_4O_5F_4$, calculations were performed using first principles. The calculated band structures with GGA showed indirect band gaps of 6.83 and 6.79 eV for α- and β-$BaB_4O_5F_4$, respectively (Fig. S7a and b, ESI†).[23] To ensure the accuracy and the consistency of the band gaps, considering the discontinuity of the exchange-related energy function, the

Table 1 The calculated Global Instability Index (GII) values for α- and β-$BaB_4O_5F_4$

	Bond valence sum				
$BaB_4O_5F_4$	Ba	B	O	F	GII
α-	2.02–2.18	2.87–3.13	1.91–2.14	0.81–1.09	0.093
β-	2.15	3.01–3.13	1.99–2.09	0.9–1.14	0.089

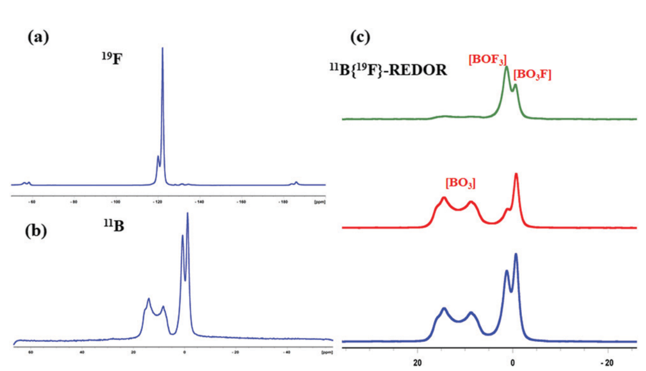

Fig. 3 ^{11}B, ^{19}F, and ^{11}B{^{19}F}-REDOR MAS NMR spectra of β-$BaB_4O_5F_4$.

Heyd–Scuseria–Ernzerhof (HSE06) hybrid DFT function was also used for the calculations.[24] According to the calculation results, the band gaps of α- and β-$BaB_4O_5F_4$ using the HSE06 function were 8.40 and 8.30 eV, respectively, meaning that the title compounds are of greater application in the DUV region. The main reasons for having large band gaps of α- and β-$BaB_4O_5F_4$ are as follows: (1) all the elements of $BaB_4O_5F_4$ are free of *d-d* or *f-f* electronic transitions; (2) the introduction of more F atoms facilitates the increase in a large band gap. In addition, in order to investigate the reasons for having a large band gap, the partial densities of states (PDOS) were calculated from the point of the intrinsic relationship between the electronic structure and the properties (Fig. S7c and d, ESI†). From −6 eV to the top of the valence band, it is dominated by O 2*p* states, F 2*p* states and B 2*p* states, whilst the bottom of the conduction band is dominated by B 2*p* states, Ba 5*d* states and a small amount of O 2*p* states. Therefore, the B–O–F and Ba–O interactions play a decisive role in determining the band gap of the title compounds. The calculated birefringence values of α- and β-$BaB_4O_5F_4$ at 1064 nm were shown to be 0.044 and 0.047, respectively, using first-principles calculations (Fig. S8, ESI†).

In summary, the first case with reversible phase transition in the fluorooxoborate family, $BaB_4O_5F_4$, has been successfully synthesized in a closed vacuum environment. It features unprecedented FBBs, $[B_{16}O_{21}F_{16}]$ in the α phase and $[B_4O_6F_4]$ in the β phase, constructing the 1D $[B_{16}O_{20}F_{16}]_\infty$ and $[B_4O_5F_4]_\infty$ chains, respectively. $BaB_4O_5F_4$ has a large band gap and moderate birefringence, indicating that it has good application prospects in the DUV region.

This work was completed with the help of the Shanghai Cooperation Organization Science and Technology Partnership Program (2020E01019), the National Natural Science Foundation of China (U2003306), the Science and Technology Service Network Initiative of CAS (KFJ-STS-QYZD-130), the Key Research Project of Frontier Science of CAS (QYZDB-SSW-JSC049) and the Fujian Institute of Innovation, CAS.

Conflicts of interest

There are no conflicts to declare.

Notes and references

1 (*a*) C. T. Chen and G. Z. Liu, *Annu. Rev. Mater. Sci.*, 1986, **16**, 203–243; (*b*) G. P. Han, Y. Wang, H. Li, Z. H. Yang and S. L. Pan, *Chem. Commun.*, 2019, **55**, 1817–1820; (*c*) X. L. Chen, B. B. Zhang, F. F. Zhang, Y. Wang, M. Zhang, Z. H. Yang, K. R. Poeppelmeier and S. L. Pan, *J. Am. Chem. Soc.*, 2018, **140**, 16311–16319; (*d*) K. M. Ok, *Acc. Chem. Res.*, 2016, **49**, 2774–2785; (*e*) T. T. Tran, H. W. Yu, J. M. Rondinelli, K. R. Poeppelmeier and P. S. Halasyamani, *Chem. Mater.*, 2016, **28**, 5238–5258.
2 C. T. Chen, B. C. Wu, A. D. Jiang and G. M. You, *Sci. Sin., Ser. B*, 1985, **28**, 235–243.
3 Y. Yang, S. L. Pan, J. Han, X. L. Hou, Z. X. Zhou, W. W. Zhao, Z. H. Chen and M. Zhang, *Cryst. Growth Des.*, 2011, **11**, 3912–3916.
4 G. Nowogrocki, N. Penin and M. Touboul, *Solid State Sci.*, 2003, **5**, 795–803.
5 M. Abudoureheman, S. J. Han, Y. Wang, Q. Liu, Z. H. Yang and S. L. Pan, *Inorg. Chem.*, 2017, **56**, 13456–13463.
6 (*a*) L. Y. Li, G. B. Li, Y. X. Wang, F. H. Liao and J. H. Lin, *Chem. Mater.*, 2005, **17**, 4174–4180; (*b*) R. E. Dinnebier, B. Hinrichsen, A. Lennie and M. Jansen, *Acta Crystallogr., Sect. B: Struct. Sci.*, 2009, **65**, 1–10; (*c*) Y. Z. Huang, L. M. Wu, X. T. Wu, L. H. Li, L. Chen and Y. F. Zhang, *J. Am. Chem. Soc.*, 2010, **132**, 12788–12789.
7 B. H. Lei, Z. H. Yang and S. L. Pan, *Chem. Commun.*, 2017, **53**, 2818–2821.
8 R. H. Cong, Y. Wang, L. Kang, Z. Y. Zhou, Z. S. Lin and T. Yang, *Inorg. Chem. Front.*, 2015, **46**, 170–176.
9 (*a*) G. Q. Shi, Y. Wang, F. F. Zhang, B. B. Zhang, Z. H. Yang, X. L. Hou, S. L. Pan and K. R. Poeppelmeier, *J. Am. Chem. Soc.*, 2017, **139**, 10645–10648; (*b*) Z. Z. Zhang, Y. Wang, B. B. Zhang, Z. H. Yang and S. L. Pan, *Angew. Chem., Int. Ed.*, 2018, **57**, 6577–6581; (*c*) X. F. Wang, Y. Wang, B. B. Zhang, F. F. Zhang, Z. H. Yang and S. L. Pan, *Angew. Chem., Int. Ed.*, 2017, **56**, 14119–14123; (*d*) Y. Wang, B. B. Zhang, Z. H. Yang and S. L. Pan, *Angew. Chem., Int. Ed.*, 2018, **57**, 2150–2154.
10 C. C. Tang, X. X. Jiang, W. L. Yin, L. J. Liu, M. J. Xia, Q. Huang, G. M. Song, X. Y. Wang, Z. S. Lin and C. T. Chen, *Dalton Trans.*, 2019, **48**, 21–24.
11 (*a*) B. B. Zhang, G. Q. Shi, Z. H. Yang, F. F. Zhang and S. L. Pan, *Angew. Chem., Int. Ed.*, 2017, **56**, 3916–3919; (*b*) M. Mutailipu, K. R. Poeppelmeier and S. L. Pan, *Chem. Rev.*, 2021, **121**, 1130–1202; (*c*) M. Mutailipu and S. L. Pan, *Angew. Chem., Int. Ed.*, 2020, **59**, 20302–20317.
12 (*a*) T. Pilz, H. Nuss and M. Jansen, *J. Solid State Chem.*, 2012, **186**, 104–108; (*b*) Y. H. Li, H. W. Yu, G. P. Han, Z. H. Yang and S. L. Pan, *Chem. Commun.*, 2019, **55**, 8923–8926; (*c*) Z. X. Lu, F. F. Zhang, A. Tudi, Z. H. Yang and S. L. Pan, *Chem. Commun.*, 2020, **56**, 15333–15336.
13 (*a*) H. W. Yu, H. P. Wu, Q. Jing, Z. H. Yang, P. S. Halasyamani and S. L. Pan, *Chem. Mater.*, 2015, **27**, 4779–4788; (*b*) X. W. Zhang, H. W. Yu, H. P. Wu, S. L. Pan, A. Q. Jiao, B. B. Zhang and Z. H. Yang, *RSC Adv.*, 2014, **4**, 13195–13200.
14 (*a*) M. Mutailipu, M. Zhang, B. B. Zhang, Z. H. Yang and S. L. Pan, *Chem. Commun.*, 2018, **54**, 6308–6311; (*b*) S. J. Han, M. Mutailipu, A. Tudi, Z. Yang and S. L. Pan, *Chem. Mater.*, 2020, **32**, 2172–2179.
15 N. E. Brese and M. O. Keeffe, *Acta Crystallogr., Sect. B: Struct. Sci.*, 1991, **47**, 192–197.
16 A. S. Sanchez, J. L. G. Munoz, J. R. Carvajal, R. S. Puche and J. L. Martinez, *J. Solid State Chem.*, 1992, **100**, 201–211.
17 Z. H. Miao, Y. Yang, Z. L. Wei, Z. H. Yang and S. L. Pan, *Inorg. Chem. Front.*, 2021, **8**, 339–343.
18 M. Q. Gai, Y. Wang, T. H. Tong, L. Y. Wang, Z. H. Yang, X. Zhou and S. L. Pan, *Chem. Commun.*, 2020, **56**, 3301–3304.
19 Z. Z. Zhang, Y. Wang, B. B. Zhang, Z. H. Yang and S. L. Pan, *Chem. – Eur. J.*, 2018, **24**, 11267–11272.
20 C. Tao and R. K. Li, *Chem. – Eur. J.*, 2020, **26**, 3709–3712.
21 (*a*) S. G. Jantz, F. Pielnhofer, L. V. Wüllen, R. Weihrich, M. J. Schäfer and H. A. Höppe, *Chem. – Eur. J.*, 2018, **24**, 443–450; (*b*) M. Mutailipu, M. Zhang, B. B. Zhang, L. Y. Wang, Z. H. Yang, X. Zhou and S. L. Pan, *Angew. Chem., Int. Ed.*, 2018, **57**, 6095–6099.
22 (*a*) T. Brauniger, T. Pilz, C. V. Chandran and M. Jansen, *J. Solid State Chem.*, 2012, **194**, 245–249; (*b*) L. J. Todd, A. R. Siedle, F. Sato, A. R. Garber, F. R. Scholer and G. D. Mercer, *Inorg. Chem.*, 1975, **14**, 1249–1252.
23 S. J. Clark, M. D. Segall, C. J. Pickard, P. J. Hasnip, M. J. Probert, K. Refson and M. C. Z. Payne, *Kristallografiya*, 2005, **220**, 567–570.
24 (*a*) J. Heyd, G. E. Scuseria and M. Ernzerhof, *J. Chem. Phys.*, 2003, **118**, 8207–8215; (*b*) A. V. Krukau, O. A. Vydrov, A. F. Izmaylov and G. E. Scuseria, *J. Chem. Phys.*, 2006, **125**, 224106.